Atmos. Chem. Phys., 22, 15413–15423, 2022
https://doi.org/10.5194/acp-22-15413-2022

Atmospheric Chemistry and Physics
Open Access
EGU

Chemical characterization of organic compounds involved in iodine-initiated new particle formation from coastal macroalgal emission

Yibei Wan[1], Xiangpeng Huang[2], Chong Xing[1], Qiongqiong Wang[1], Xinlei Ge[2], and Huan Yu[1]

[1]School of Environmental Studies, China University of Geosciences, Wuhan 430074, China
[2]Jiangsu Key Laboratory of Atmospheric Environment Monitoring and Pollution Control, Collaborative Innovation Center of Atmospheric Environment and Equipment Technology, School of Environmental Science and Engineering, Nanjing University of Information Science and Technology, Nanjing 210044, China

Correspondence: Huan Yu (yuhuan@cug.edu.cn)

Received: 26 August 2022 – Discussion started: 1 September 2022
Revised: 31 October 2022 – Accepted: 11 November 2022 – Published: 6 December 2022

Abstract. Iodine-initiated new particle formation (I-NPF) has long been recognized in coastal hotspot regions. However, no prior work has studied the exact chemical composition of organic compounds and their role in coastal I-NPF. Here we present an important complementary study to the ongoing laboratory and field research on iodine nucleation in the coastal atmosphere. Oxidation and NPF experiments with vapor emissions from real-world coastal macroalgae were simulated in a bag reactor. On the basis of comprehensive mass spectrometry measurements, we reported for the first time a variety of volatile precursors and their oxidation products in gas and particle phases in such a highly complex system. Organic compounds overwhelmingly dominated over iodine in the new particle growth initiated by iodine species. The identity and transformation mechanisms of organic compounds were proposed in this study to provide a more complete story of coastal NPF from low-tide macroalgal emission.

1 Introduction

Coastal new particle formation (NPF) may be driven by daytime low-tide emission of iodine species from macroalgae fully or partially exposed to the air. The phenomenon was reported in hotspot locations of west Europe, Australia and polar regions (O'Dowd et al., 2002; Heard et al., 2006; McFiggans et al., 2010; Whitehead et al., 2009; Sipilä et al., 2016; Allan et al., 2015; Baccarini et al., 2020; Beck et al., 2021). On the southeast coastline of China, we reported intense iodine-initiated NPF based on particle number size distribution and iodine measurements (Yu et al., 2019).

To simulate iodine-initiated NPF (I-NPF) in controlled laboratory conditions, I_2 or CH_2I_2 vapor was usually photolyzed in the presence of ozone to provide nucleation precursors (Burkholder et al., 2004; Jimenez et al., 2003; Monahan et al., 2012; Saunders and Plane, 2005; O'Dowd et al., 2004; Gómez Martín et al., 2020; He et al., 2021; Huang et al., 2022; Gómez Martín et al., 2022). Ashu-Ayem et al. (2012), Monahan et al. (2012), McFiggans et al. (2004), Sellegri et al. (2005) and Sellegri et al. (2016) also investigated NPF from the vapors emitted by real-world macroalgal specimens or seawater in laboratory chamber or apparatus. However, the focus of all the above studies was emission rate, oxidation mechanisms or nucleation pathways of iodine species. For example, positive correlations between particle concentrations and I_2 or CH_2I_2 mixing ratios were usually observed (Burkholder et al., 2004; Jimenez et al., 2003; Sellegri et al., 2005; Monahan et al., 2012). Kinetic studies in a flow tube or a CERN CLOUD chamber proposed the clustering of iodine oxides (I_xO_y) or iodine oxoacids (HIO_3, HIO_2) as nucleation mechanisms on the basis of photoionization time-of-flight mass spectrometry (TOF-MS; Gómez Martín et al., 2020), atmospheric pressure interface TOF (APi-TOF)

and nitrate chemical ionization mass spectrometer (nitrate-CIMS) measurements (He et al., 2021; Gómez Martín et al., 2022).

Organic compounds have also been suggested to be involved in coastal NPF (Vaattovaara et al., 2006; Yu et al., 2019). Huang et al. (2022) and Saunders et al. (2010) investigated the effect of uptake of meso-erythritol, glyoxal, dimethylamine and oxalic acid on the growth of iodine oxide nanoparticles. However, no prior work has investigated the exact chemical identity of organic compounds (other than iodomethane) and their role in I-NPF. The role of biogenic terpenes and anthropogenic aromatics in continental NPF has been recognized for a long time (Donahue et al., 2013). Their ozonolysis or photochemistry products have been investigated in depth using electrospray ionization mass spectrometry (ESI-MS) and, more recently, CIMS instruments (Nguyen et al., 2010; Kundu et al., 2017, 2012; Faxon et al., 2018; Wang et al., 2020; Riva et al., 2017; Yan et al., 2020; Ehn et al., 2014). It is very likely that certain volatile organic compounds (VOCs) emitted mutually with iodine or iodinated methane from coastal biota or biologically active sea surface may also be involved in the coastal I-NPF process and promote the growth of iodine particles.

To test this hypothesis, we conducted oxidation and NPF experiments with vapor emissions from real-world coastal macroalgae in a bag reactor. A suite of mass spectrometric methods including inductively coupled plasma MS (ICP-MS), gas chromatography MS (GC-MS), iodide-CIMS and ESI-orbitrap MS were applied to measure vapor precursors, gaseous products and particulate products during the NPF process. Mass concentrations of total organic carbon (TOC) and total iodine (TI) of new particles were compared to evaluate the relative importance of organics and iodine in new particle growth. The identity and transformation mechanisms of organic compounds were identified to provide a more complete story of coastal NPF from low-tide macroalgal emission. Our study is thus complementary to prior laboratory and field studies of I-NPF but has an emphasis on organics.

2 Experiments

2.1 Experimental apparatus and sample collection

Similar to a potential aerosol mass (PAM) oxidation flow reactor, a bag reactor was designed to provide an oxidizing environment for simulating atmospheric oxidation processes of algae-emitted VOCs. The bag reactor was made from 75 µm thick fluorinated ethylene propylene (FEP) Teflon (1.2 m × 1.5 m, flat dimension). The volume of the bag at full inflation was determined experimentally to be about 200 L. The bag was suspended vertically (Fig. 1) and kept in the dark or directly exposed to room light of a fluorescent lamp. Before each experiment, the bag was purged for several hours to reduce background particle concentrations to below 1 cm^{-3}.

Undaria pinnatifida, a common brown seaweed species found in the Xiangshan Gulf on the east China coast, was collected from local intertidal zone and stored at −10 °C until the experiments. A quantity of 2 kg macroalgae was put in a 20 L Pyrex glass bottle that was filled with ∼ 1 L natural seawater. The specimens were partially exposed to the air to simulate tidal emersion of macroalgae. A flow of particle-free ultra-high-purity (UHP) air blew algae-emitted VOCs out of the bottle and merged with a diluting air flow before entering the bag reactor.

Two types of experiments were conducted. In the three ozonolysis experiments, ozone (O_3) was generated by UHP air flowing through a 5 W 185 nm UV lamp. The O_3 flow was fed just before the bag reactor was fully inflated. Final O_3 concentration in the bag reactor was measured to be ∼ 500 ppbv using an ozone analyzer (Model 49i, Thermo-Fisher Scientific Inc.). RH was estimated to be 10 % in the bag reactor assuming 0.3 L min^{-1} water-saturated VOC flow was diluted by 2.7 L min^{-1} dry-air flow. In an additional OH-enhanced experiment, the O_3 / VOC mixture flow was directed through a 254 nm UV light before entering the bag reactor. OH radicals were produced via the reaction $O_3 + h\nu \rightarrow O_2 + O(^1D)$ and $O(^1D) + H_2O \rightarrow 2OH$. Integrated OH exposure time was determined by a SO_2 decay experiment to be 2.4 d in the experimental apparatus assuming an ambient average OH concentration of 1.5×10^6 molecules cm^{-3} (see Supplement Sect. S1). Other oxidants may include $O(^3P)$ that resulted from the quenching of $O(^1D)$ (Li et al., 2015). Because the purpose of this study is to identify gas and particle products of algae-emitted VOCs in the simulated NPF event, a significantly higher oxidation level in the bag reactor than the atmosphere should not change the conclusions in the article. Wall loss, aerosol yield, reaction rate and other kinetic factors in the bag reactor were also not evaluated.

The bag reactor was first operated in a static mode to monitor the time evolution of gaseous products and particle size. In the static mode, the bag was first filled to full inflation with the VOC / O_3 flows. The flows were then shut down; a scanning mobility particle sizer (SMPS; model 3936, TSI Inc., Shoreview, MN, USA) and an Aerodyne iodide-CIMS pulled two flows of 0.3 and 1.8 L min^{-1} out of the bag, respectively. The SMPS measured the particle number size distribution from 14 to 600 nm.

The bag reactor was then operated in a dynamic mode for a few hours to collect enough particles for offline chemical analysis. In the dynamic mode, the VOC / O_3 flow of 3 L min^{-1} was fed to the bag continuously, while the SMPS and a vacuum pump (GAST Group Ltd.) pulled sample flows of 0.3 and 2.7 L min^{-1}, respectively, out of the bag reactor. This resulted in an overall residential time of 67 min for the O_3 / VOC mixture in the fully inflated bag. The particles in the 2.7 L min^{-1} sample flow were collected onto a Zefluor®

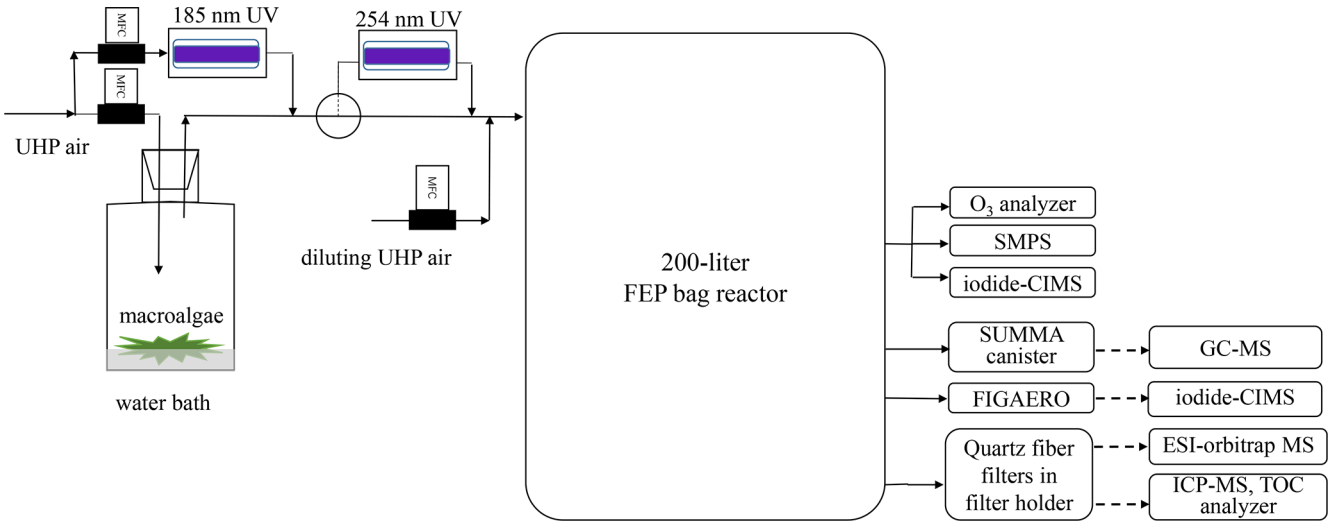

Figure 1. Schematic of experimental setup. Solid line: air flows. Dashed lines: sent for offline chemical analysis.

PTFE membrane filter mounted in a filter inlet for gases and aerosols (FIGAERO) for iodide-CIMS analysis or, alternatively, onto 47 mm diameter double quartz fiber filter pack mounted in a filter holder for ESI-orbitrap MS, ICP-MS and TOC analysis. The front filter of the double-filter pack collected the particles and also adsorbed some volatile species as positive artifacts, while the back filter placed downstream of the front filter was supposed to adsorb the same amount of volatile species as the front filter.

2.2 Chemical analysis

Before the ozonolysis experiments, the algae-emitted VOCs in the bag reactor were collected by a 6 L pre-evacuated stainless-steel canister (Entech Instruments, Inc., Simi Valley, CA, USA) and analyzed using a quadrupole GC-MS system (model TH-300B, Wuhan Tianhong Instruments Co. Ltd., Wuhan, China). The algae-emitted VOCs, as well as their gaseous and particulate products, were also measured by the FIGAERO-iodide-CIMS. Iodide-adduct chemical ionization is well suited for measuring oxygenated or acidic compounds with minimal fragmentation. More details of the GC-MS and FIGAERO-iodide-CIMS measurements can be found in Sect. S2. The theory and design of the two instruments were described by Wang et al. (2014) and Lopez-Hilfiker et al. (2014).

The particles collected on quartz fiber filters were sent for offline quantification of TOC and TI, as well as nontarget analysis of organic compounds using ESI-orbitrap MS. The front and back filters were treated, separately, following the procedure as below: the filter was ultrasonicated twice with 10 mL water and acetone nitrile solvent mixture ($v : v = 1 : 1$). Ultrasonication time and power were 20 min and 150 W. The extract was filtered by a 0.2 µm PTFE syringe filter and evaporated in a rotary evaporator to 0.5 mL. After being centrifuged for 30 min at 12 000 rpm, the supernatant was collected for TI analysis by Agilent 1100 HPLC-7900 ICP-MS (Agilent Technologies, Santa Clara, CA, USA) and TOC analysis by a TOC analyzer (Model TOC-5000A, Shimadzu, Japan). TI or TOC in the particles was obtained by subtracting the amount on the back filter from that on the front filter. Nontarget analysis of organic compounds in the supernatant was conducted using a Q Exactive hybrid Quadrupole-Orbitrap mass spectrometer (Thermo Scientific, Bremen, Germany). The supernatant was directly infused by a syringe pump and ionized in negative ESI source. All the ions in the m/z range from 50 to 500 Th were scanned with a mass resolution of 70 000. The chemically sound CHO molecular formulas were computed with a mass tolerance of ±2 ppm for these ions. Only the compounds that existed solely in the front filter or with ion intensity in the front filter higher than that in the back filter by a factor of 3 were regarded as the organic compounds in the particle phase (Wang et al., 2017).

3 Results and discussion

No particles formed in the absence of room light or O_3 (see Supplement Fig. S1). Therefore, light was on throughout the experiments reported in the article. In the static mode experiments, we could not observe gas-phase products until 48 min after O_3 injection. New particles larger than 14 nm were observed only 58 min after O_3 injection. Afterwards, new particles began to grow to form a typical banana-shape particle size spectrum (Fig. 2a). This relatively long waiting time was likely due to the buildup of O_3 and oxidation products. Time zero of Fig. 2 was thus set as the time when gaseous products first appeared.

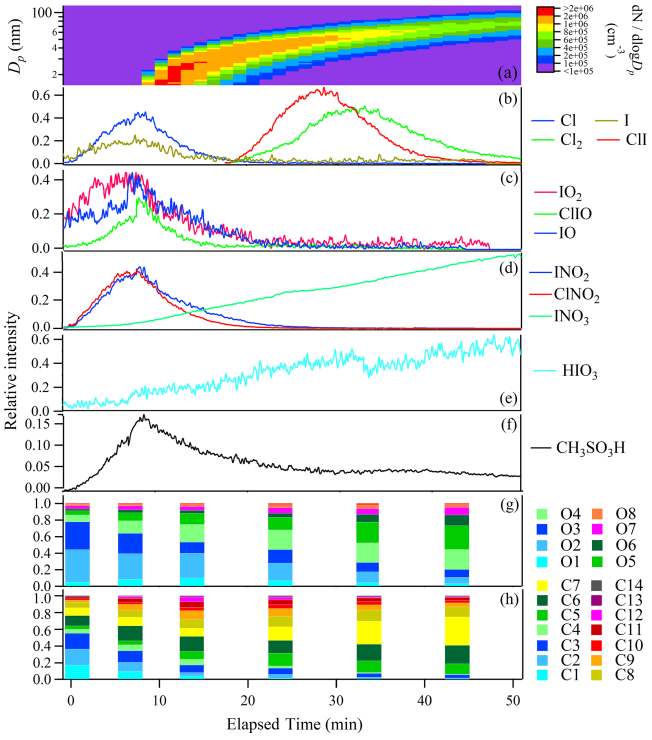

Figure 2. Time evolution of particle number size distribution **(a)** and relative intensities of gaseous molecules and radicals **(b–f)**; the fractions of organic compounds grouped by O and C atom numbers in the selected time points **(g–h)** in a typical ozonolysis experiment (static mode). Time zero was set as the time when gaseous products first appeared.

3.1 Macroalgal emission

It is of particular interest to know what VOCs are emitted from coastal macroalgae. They are potential precursors of iodine particle nucleation and growth. The canister sampling followed by GC-MS analysis showed that the top nine non-CHO compounds with highest TIC (total ion chromatogram) peak areas (Table 1) are C_5 alkanes, C_{10} α-pinene, and halogenated C_1, C_3 and C_5 alkanes. The top 10 CHO compounds are C_2–C_6 alcohols and carbonyls with saturated or unsaturated carbon chain.

The iodide-CIMS is more sensitive to more oxygenated or acidic compounds and thus complementary to the GC-MS measurement. The 76 organic precursors detected by the iodide-CIMS before ozone addition were characterized by $C_{1,2,3,6}$ and O_{2-3} formulas (Fig. 3a). The top seven compounds with highest ion intensities were CH_2O_2, $C_2H_4O_2$, $C_3H_6O_3$, $C_6H_{10}O_3$, $C_2H_6O_2$, $C_4H_8O_2$ and $C_6H_{12}O_3$, which accounted for 82.5 % of total ion intensity. They are C_1–C_6 mono-carboxylic acids, hydroxyl carboxylic acids or oxo-carboxylic acids with two to three oxygen atoms (Table 1). Their carbon atom numbers are in general consistent with the VOCs detected by GC-MS.

Table 1. Major volatile organic compounds emitted by macroalgae as potential NPF precursors, sorted by TIC peak area measured by GC/MS or MS peak intensity measured by the iodide-CIMS.

	Formula	Structure	Peak area/MS peak intensity
		GC/MS, non-CHO compounds	
1	C_5H_{12}		1.90×10^6
2	C_5H_{10}		1.59×10^6
3	CH_3I		1.37×10^6
4	C_3H_7I		7.60×10^5
5	$CHBr_3$		4.71×10^5
6	$C_5H_{11}I$		3.75×10^5
7	$CHBr_2Cl$		2.71×10^5
8	CH_2Cl_2		2.55×10^5
9	$C_{10}H_{16}$		2.26×10^5
		GC/MS, CHO compounds	
1	C_2H_6O		1.70×10^7
2	C_3H_6O		1.38×10^7
3	$C_4H_6O_2$		1.30×10^7
4	$C_6H_{12}O$		1.03×10^7
5	$C_5H_{10}O$		1.00×10^7
6	$C_4H_{10}O$		5.16×10^7
8	C_2H_4O		3.46×10^7
9	$C_6H_{10}O$		2.88×10^7
7	C_5H_8O		1.45×10^7
10	C_4H_8O		1.37×10^7
		Iodide-CIMS	
1	CH_2O_2		1.58×10^6
2	$C_2H_4O_2$		9.52×10^5
3	$C_3H_6O_3$		9.21×10^5
4	$C_6H_{10}O_3$		4.44×10^5
5	$C_2H_6O_2$		2.88×10^5
6	$C_4H_8O_2$		1.17×10^5
7	$C_6H_{12}O_3$		1.12×10^5

Relatively high signals of NO_3^- and HNO_3I^- were observed before the addition of ozone to the bag reactor. They were likely HNO_3 or nitrate vaporized from algal specimens or natural seawater. Because NO_3^- and HNO_3I^- were also observed in the particle phase during the NPF (Fig. 4), we

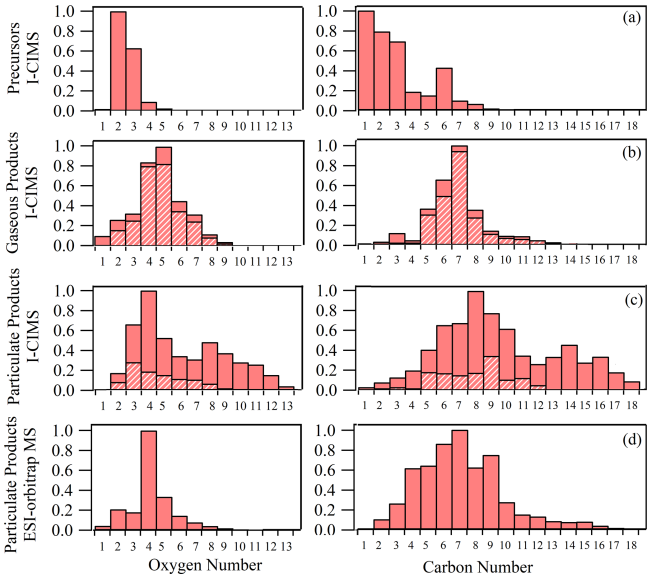

Figure 3. Oxygen and carbon atom number distributions of potential VOC precursors **(a)**, gaseous products **(b)** and particulate products measured by the iodide-CIMS **(c)**, as well as the particulate products measured by ESI-orbitrap MS **(d)** in a typical ozonolysis experiment (dynamic mode). Hatched bars indicate the fractions of organic formulas observed in both gas and particle phases by the iodide-CIMS.

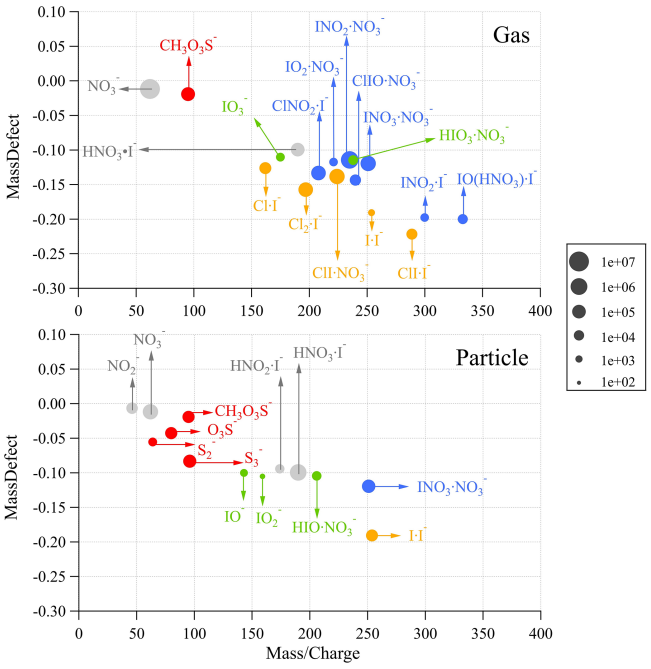

Figure 4. Integrated ion intensities of inorganic molecules and radicals in the gas phase (static mode) and particle phase (dynamic mode) measured by the iodide-CIMS in a typical ozonolysis experiment. The ions were color-coded according to their elemental composition. For each ion cluster, the parent neutral molecule is on the left-hand side of the middle dot, while the clustering ion I^- or NO_3^- is on the right-hand side. Those without a clustering ion are shown as bare anions.

assume HNO_3 was also an important precursor of particle formation.

3.2 Gaseous products

3.2.1 Gaseous inorganic molecules and radicals

Being different from the nitrate-CIMS, our iodide-CIMS did not detect nucleating clusters of iodine oxides or oxyacids after the addition of ozone. Instead, dozens of new inorganic molecules or radicals were observed as clusters with I^-, NO_3^- or deprotonated ions in the gas or particle phase (Fig. 4). We grouped these species by elemental composition and investigated their role in the NPF by observing how their gaseous ion intensities evolved during the NPF event in the bag reactor (Fig. 2b–f).

1. *Cl, I, Cl_2 and ClI in the gas phase*. The intensities of I and Cl increased ca. 10 min before 14 nm particles appeared and decreased as the particles grew up (Fig. 2b). Based on prior work of Burkholder et al. (2004), Jimenez et al. (2003) and O'Dowd et al. (2004), we suggested the photolysis of CH_2Cl_2, CHBrCl, CH_3I and C_3H_7I was the source of halogen atoms (e.g., $CH_3I + h\nu \rightarrow CH_3 + I$), although we could not exclude the photolysis of other precursors like I_2 and HOI that are invisible to GC-MS and the iodide-CIMS. There was a time lag of 20–25 min between the appearances of Cl and I and those of ClI and Cl_2, which probably resulted from anion exchange reactions of $Cl \cdot I^-$ and $I \cdot I^-$ with Cl atoms.

2. *IO_2, IO and ClIO in the gas phase*. These species showed a similar time evolution to I and Cl atoms (Fig. 2c). They could be from the reactions between I, ClI and O_3 (Saiz-Lopez et al., 2014). Sequential oxidation and aggregation reactions might have formed other halogen oxides (Gómez Martín et al., 2013), but they might not be detectable by the iodide-CIMS.

3. *INO_2, $ClNO_2$ and INO_3*. INO_2 and $ClNO_2$ were detected in the gas phase with similar time evolution with halogen atoms and halogen oxides (Fig. 2d). INO_3 was found in both gas and particle phases. INO_2 and INO_3 were usually thought to form upon the reactions $I + NO_2 + M \rightarrow IONO + M$ and $IO + NO_2 + M \rightarrow IONO_2 + M$ in the atmosphere (Saiz-Lopez et al., 2012), which seems to be unlikely in our bag reactor because NO_2 was not added. Considering NO_3^- was ubiquitous in the bag reactor of our experiment, it is likely that INO_2 and INO_3 formed via $I_2O_2 + NO_3^- \rightarrow IO_3^- + IONO$ and $I_2O_3 + NO_3^- \rightarrow IO_3^- + IONO_2$. These reaction pathways have been supported by theoretical calculation

and flow tube mass spectrometry experiments (Gómez Martín et al., 2022, 2020). $ClNO_2$ was likely to form upon similar reaction between Cl_2O_2 and NO_3^- in the bag reactor.

4. *HIO, HIO_2 and HIO_3*. HIO_3 seems to be the end product of the above intermediates because its gas-phase ion intensity kept on increasing during new particle growth (Fig. 2e). Based on this fact, we assume that HIO_3 could be from $I_2O_5 + H_2O \rightarrow 2HIO_3$ or $I_2O_y + NO_3^- \rightarrow IO_3^- + INO_y$. On the other hand, HIO_3 was not detected in the particle phase by the iodide-CIMS, which is contrary to the offline analysis of the quartz filter by HPLC-ICP-MS showing that total iodine was mostly dominated by IO_3^- peak. We speculate that HIO_3 might have been dehydrated to I_2O_5 under thermal desorption temperature up to 180 °C in FIGAERO. The signals of IO^-, IO_2^- and $HIONO_3^-$ (corresponding to HIO and HIO_2) were found in the particle phase but not in the gas phase. He et al. (2021) proposed HIO_2 formation via $I^- + H_2O + O_3 \rightarrow HIO_2$ or $I_2O_2 + H_2O \rightarrow HIO + HIO_2$. With limit experimental evidence of our work, the exact formation pathways of HIO_x remain to be explored in future.

5. *CH_3SO_3H, S_2^-, S_3^- and SO_3^-*. We observed methane sulfonic acid (CH_3SO_3H, MSA) in both gas and particle phases. Gaseous MSA increased in the beginning but decreased after new particles appeared (Fig. 2f). Apparently, our measurement suggested MSA contributed to the growth of new particles, but it is unknown if it also participated in nucleation. We suggested S_2^-, S_3^- and SO_3^- ions observed in the particle phase were thermal decomposition products of MSA.

We note that CH_3I vapor was added as an ion source reagent to the ion molecule reactor (IMR) of the iodide-CIMS. It is likely that this extra CH_3I in the IMR might obscure the interpretation of the observed iodine containing clusters. We believed that the ion source reagent CH_3I should have relatively small interference with inorganic iodine compounds from the bag reactor, on the basis of two facts: (1) the ion source reagent CH_3I was added directly from the permeation tube into the IMR. Without photolysis, the ion source reagent CH_3I in the IMR should not become a source of I and I_xO_y. (2) The concentration of the ion source reagent CH_3I and its potential products should be quite constant as long as O_3 was present in the IMR, which was not supported by the variable signals of I, ClI, IO_2, IO, ClIO, HIO_3, INO_2 and INO_3 in Fig. 2.

3.2.2 Gaseous organic products

After ozone addition, a gradual transformation from C_1–C_3 precursors to C_5–C_8 gaseous products was observed during the NPF process (Fig. 2h). In the meanwhile, the oxygen

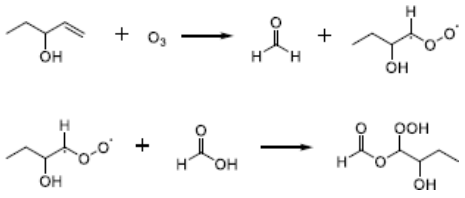

Scheme 1. A proposed addition reaction involving stabilized Criegee intermediates in the gas phase.

atom number of the compounds increased from two–three to four–seven (Fig. 2g). The formation of compounds with more carbon atoms than the parent VOCs is unlikely in the gas phase, except bimolecular reactions of stabilized Criegee intermediates (SCIs) that typically form upon alkene ozonolysis. Similar to isoprene ozonolysis (Riva et al., 2017; Inomata et al., 2014), we propose the SCI addition mechanism can also explain the transformation observed in our case: (1) C_4 SCIs formed upon the ozonolysis of CHO precursors with C=C double bonds (e.g., those observed by GC-MS in Table 1), and (2) the insertion of C_4 SCIs into carboxylic acid precursors (e.g., those observed by the CIMS in Table 1) produced oligomeric hydroperoxides. An example is shown in Scheme 1 for the reactions of most abundant ethyl vinyl carbinol ($C_5H_{10}O$), ozone and formic acid (CH_2O_2), but the same mechanism is also applicable for ethyl vinyl ketone (C_5H_8O) and other abundant C_2–C_5 carboxylic acids and hydroxyl carboxylic acids. As a result, a series of gaseous oligomeric hydroperoxides, $C_5H_{10}O_5$, $C_6H_{10}O_5$, $C_6H_{12}O_5$, $C_7H_{12}O_6$, $C_7H_{14}O_6$, $C_8H_{14}O_5$, $C_8H_{16}O_6$, $C_8H_{16}O_5$ and $C_9H_{16}O_6$, were observed with high intensity by the iodide-CIMS.

3.3 Particulate products

3.3.1 Relative mass contribution of organic carbon and iodine to new particles

In the dynamic-mode experiments, O_3 in the bag reactor was kept at its maximum concentration of 200 ppbv. With a prolonged residential time of 67 min, the particles grew to 102 ± 23 nm, which was measured by the SMPS at the outlet of the bag reactor. The TOC and TI measurements show that organic compounds contributed more particle mass than iodine, with a TOC / (I + TOC) ratio of 96.1 ± 2.9 % (Table 2).

In the OH-enhanced experiment (dynamic mode), more particulate products were generated with enhanced oxidation capacity: TI in the particles increased by a factor of 10.8, TOC increased by a factor of 2.7 and particle number concentration increased by a factor of 7.4. On the other hand, particle size decreased to 73 nm, and the TOC / (TI + TOC) ratio decreased to 92.9 % (Table 2). These differences indicate that more iodine nuclei were produced with enhanced oxidation capacity, probably via $OIO + OH \rightarrow HOIO_2$ (Plane et al., 2006) and $O(^3P) + CH_3I \rightarrow IO + CH_3$ (Teruel et al.,

Table 2. Particle number concentration (N), mean diameter (D_p), total organic carbon (TOC) and total iodine (TI) of new particles with a residential time of 67 min in the bag reactor in the ozonolysis experiments and OH-enhanced experiment (dynamic mode). Those of 10–56 nm new particles collected by a nano micro-orifice uniform deposit impactor (nano-MOUDI; MSP, Inc.) during an I-NPF event at a coastal site of Ningbo, China (Yu et al., 2019), are also listed.

	TOC ($\mu g\,m^{-3}$)	TI ($\mu g\,m^{-3}$)	TOC / (TI + TOC)	N (cm^{-3})	D_p (nm)
Ozonolysis experiments	45.6 ± 9.7	0.88 ± 0.34	$96.1 \pm 2.9\,\%$	$(5.58 \pm 2.04) \times 10^4$	102 ± 23
OH-enhanced experiment	125.3	9.5	92.9 %	4.16×10^5	73
I-NPF event at a coastal site of China	0.7	0.0135	98.2 %	6.00×10^5	16

2004). Competitive uptake of condensing organic vapors onto these iodine nuclei limited the growth of individual new particles. Nevertheless, organic compounds overwhelmingly dominated over iodine in the mass contribution to new particle growth.

The significant organic contribution observed in the laboratory condition is generally consistent with the TOC / (I+TOC) ratio of 98.2 % in 10–56 nm new particles collected during a coastal I-NPF event in China (Yu et al., 2019), although TOC and TI during the field event are 2 orders of magnitude lower than those in the bag reactor (Table 2). The mean diameter of new particles was observed to be only 16 nm during the field event. But those small new particles are expected to grow into cloud condensation nuclei (CCN) active sizes, given longer residence time and uptake of more condensing vapors in the atmosphere (He et al., 2021).

3.3.2 Particulate organic products

In the end of a typical ozonolysis experiment (dynamic mode), 100 and 364 new formulas were observed in the gas and particle phases, respectively, including 73 semivolatile organic compounds (SVOCs) that appeared in both gas and particle phases. Those SVOCs accounted for 81 % and 20 % of total ion intensities of gaseous and particulate products, respectively. Being different from unimodal atom number distributions of gaseous products ($C_{max} = 7$ and $O_{max} = 5$, Fig. 3b), particulate products were characterized by distinct bimodal or trimodal distribution of carbon number ($C_{max} = 8$, 14 and 16, Fig. 3c) and oxygen number ($O_{max} = 4$ and 8), implying possible dimer formation via accretion reactions in the particle phase.

ESI-Orbitrap MS differs from the FIGAERO-iodide-CIMS in its extraction method (ultrasonic solvent extraction from quartz fiber filter vs. thermal desorption from PTFE membrane filter), ionization source (electrospray ionization vs. iodide-adduct chemical ionization) and MS-resolving power (70 000 vs. 4500). The result showed that ESI-orbitrap MS and the FIGAERO-iodide-CIMS detected 336 and 364 organic formulas, respectively, in the particle phase. A total of 167 organic formulas were commonly observed by both methods, which accounted for 87 % and 54 % of total ion intensity of organic formulas by the two methods, respectively (Fig. S2). As shown in Fig. 3c and d, the FIGAERO-iodide-CIMS had better sensitivity toward the organic compounds with more oxygen atoms (e.g., $O \geq 8$) and carbon atoms (e.g., $C \geq 10$). As a result, bimodal carbon and oxygen atom number distributions were observed by the FIGAERO-iodide-CIMS but not ESI-orbitrap MS.

The measurement by ESI-orbitrap MS provided more insights about the formation mechanism of particulate products. We compared the 336 formulas detected by ESI-orbitrap MS in our study with the 414 formulas of isoprene ozonolysis secondary organic aerosol (SOA) products (Nguyen et al., 2010) and 922 formulas of α-pinene ozonolysis SOA products (Putman et al., 2012) measured by the ESI-orbitrap MS. It was found that 72 % of the formulas in this study can also be found in isoprene SOA, but only 39 % can be found in α-pinene SOA. This seems to imply that some similar alkene ozonolysis reactions occurred in our system and isoprene ozonolysis.

For such a highly complex system full of various algae-emitted precursors, it is impossible to simply propose a reaction mechanism to explain the formation of all particulate products, nor to list all reactions occurring in the bag reactor. On the basis of particle-phase oligomer chemistry (Seinfeld and Pandis, 2016), especially the well-understood isoprene ozonolysis SOA chemistry (Nguyen et al., 2010; Inomata et al., 2014; Riva et al., 2017), we suggest that a variety of accretion reactions without uniform oligomerization pattern (e.g., esterification, aldol condensation, hemiacetal reactions, peroxyhemiacetal formation and SCI reactions) transformed $O_{max} = 4$ and $C_{max} = 8$ multifunctional monomers (like alcohols, carbonyls, hydroperoxides and carboxylic acids) to $O_{max} = 8$ and $C_{max} = 14$ or 16 dimers. As an example, we used two simplified reaction equations to illustrate addition-type cross-oligomerization between C_6 and C_8 monomers

and self-oligomerization of C_8 monomers, respectively:

$$C_6H_{6-12}O_{3-6} + C_8H_{10-16}O_{3-6}\cdot \rightarrow C_{14}H_{16-26}O_{6-12}$$
$$C_8H_{10-16}O_{3-6} + C_8H_{10-16}O_{3-6}\cdot \rightarrow C_{16}H_{20-32}O_{6-12},$$

in which the C_6 , C_8, C_{14} and C_{16} formulas in the equations are among the most abundant ones observed in the particle phase by the iodide-CIMS.

4 Conclusions

Using a suite of mass spectrometers, we reported, for the first time, the chemical compositions of volatile precursors emitted by real-world coastal macroalgae and their gaseous and particulate oxidation products. In the presence of room light and ozone, the photolysis of halogenated $C_{1,3,5}$ alkanes ends up as HIO_3 and INO_3. It was most likely HIO_3 initiated NPF and provided nuclei for the further condensation of other products like MSA and CHO compounds. Gas-phase SCI reactions and particle-phase accretion reactions transformed C_1–C_6 and O_2–O_3 precursors gradually to particulate products with $C_{max} = 8$, 14 and 16 and $O_{max} = 4$ and 8. As a result, organic carbon was found to overwhelmingly dominate over iodine in the mass contribution to the new particle growth. Although our instruments did not allow for the detection of nucleating clusters of iodine oxides or oxyacids, our study provided important complementary information to the ongoing laboratory and field research on coastal I-NPF.

Data availability. All data related to figures and tables in this study have been archived and are available through the Zenodo data repository at https://doi.org/10.5281/zenodo.6965859 (Yu, 2022).

Supplement. The supplement related to this article is available online at: https://doi.org/10.5194/acp-22-15413-2022-supplement.

Author contributions. HY designed the experiment. YW, XH and CX conducted the experiments. YW and HY analyzed the data and wrote the manuscript. QW and XG reviewed and revised the manuscript.

Competing interests. The contact author has declared that none of the authors has any competing interests.

Disclaimer. Publisher's note: Copernicus Publications remains neutral with regard to jurisdictional claims in published maps and institutional affiliations.

Financial support. This work was supported by the National Science Foundation of China (grant nos. 41975831 and 42175131) and start-up research funding from the China University of Geosciences.

Review statement. This paper was edited by James Allan and reviewed by two anonymous referees.

References

Allan, J. D., Williams, P. I., Najera, J., Whitehead, J. D., Flynn, M. J., Taylor, J. W., Liu, D., Darbyshire, E., Carpenter, L. J., Chance, R., Andrews, S. J., Hackenberg, S. C., and McFiggans, G.: Iodine observed in new particle formation events in the Arctic atmosphere during ACCACIA, Atmos. Chem. Phys., 15, 5599–5609, https://doi.org/10.5194/acp-15-5599-2015, 2015.

Ashu-Ayem, E. R., Nitschke, U., Monahan, C., Chen, J., Darby, S. B., Smith, P. D., O'Dowd, C. D., Stengel, D. B., and Venables, D. S.: Coastal Iodine Emissions. 1. Release of I_2 by Laminaria digitata in Chamber Experiments, Environ. Sci. Technol., 46, 10413–10421, https://doi.org/10.1021/es204534v, 2012.

Baccarini, A., Karlsson, L., Dommen, J., Duplessis, P., Vüllers, J., Brooks, I. M., Saiz-Lopez, A., Salter, M., Tjernström, M., Baltensperger, U., Zieger, P., and Schmale, J.: Frequent new particle formation over the high Arctic pack ice by enhanced iodine emissions, Nat. Commun., 11, 4924, https://doi.org/10.1038/s41467-020-18551-0, 2020.

Beck, L. J., Sarnela, N., Junninen, H., Hoppe, C. J. M., Garmash, O., Bianchi, F., Riva, M., Rose, C., Peräkylä, O., Wimmer, D., Kausiala, O., Jokinen, T., Ahonen, L., Mikkilä, J., Hakala, J., He, X.-C., Kontkanen, J., Wolf, K. K. E., Cappelletti, D., Mazzola, M., Traversi, R., Petroselli, C., Viola, A. P., Vitale, V., Lange, R., Massling, A., Nøjgaard, J. K., Krejci, R., Karlsson, L., Zieger, P., Jang, S., Lee, K., Vakkari, V., Lampilahti, J., Thakur, R. C., Leino, K., Kangasluoma, J., Duplissy, E.-M., Siivola, E., Marbouti, M., Tham, Y. J., Saiz-Lopez, A., Petäjä, T., Ehn, M., Worsnop, D. R., Skov, H., Kulmala, M., Kerminen, V.-M., and Sipilä, M.: Differing Mechanisms of New Particle Formation at Two Arctic Sites, Geophys. Res. Lett., 48, e2020GL091334, https://doi.org/10.1029/2020GL091334, 2021.

Burkholder, J. B., Curtius, J., Ravishankara, A. R., and Lovejoy, E. R.: Laboratory studies of the homogeneous nucleation of iodine oxides, Atmos. Chem. Phys., 4, 19–34, https://doi.org/10.5194/acp-4-19-2004, 2004.

Donahue, N. M., Ortega, I. K., Chuang, W., Riipinen, I., Riccobono, F., Schobesberger, S., Dommen, J., Baltensperger, U., Kulmala, M., Worsnop, D. R., and Vehkamaki, H.: How do organic vapors contribute to new-particle formation?, Faraday Discuss., 165, 91–104, https://doi.org/10.1039/C3FD00046J, 2013.

Ehn, M., Thornton, J. A., Kleist, E., Sipila, M., Junninen, H., Pullinen, I., Springer, M., Rubach, F., Tillmann, R., Lee, B., Lopez-Hilfiker, F., Andres, S., Acir, I.-H., Rissanen, M., Jokinen, T., Schobesberger, S., Kangasluoma, J., Kontkanen, J., Nieminen, T., Kurten, T., Nielsen, L. B., Jorgensen, S., Kjaergaard, H. G., Canagaratna, M., Maso, M. D., Berndt, T., Petaja, T., Wahner, A., Kerminen, V.-M., Kulmala, M., Worsnop, D. R., Wildt, J., and Mentel, T. F.: A large source of low-volatility secondary organic aerosol, Nature, 506, 476–479, https://doi.org/10.1038/nature13032, 2014.

Faxon, C., Hammes, J., Le Breton, M., Pathak, R. K., and Hallquist, M.: Characterization of organic nitrate constituents of secondary organic aerosol (SOA) from nitrate-radical-initiated oxidation of limonene using high-resolution chemical ioniza-

tion mass spectrometry, Atmos. Chem. Phys., 18, 5467–5481, https://doi.org/10.5194/acp-18-5467-2018, 2018.

Gómez Martín, J. C., Gálvez, O., Baeza-Romero, M. T., Ingham, T., Plane, J. M. C., and Blitz, M. A.: On the mechanism of iodine oxide particle formation, Phys. Chem. Chem. Phys., 15, 15612–15622, https://doi.org/10.1039/c3cp51217g, 2013.

Gómez Martín, J. C., Lewis, T. R., Blitz, M. A., Plane, J. M. C., Kumar, M., Francisco, J. S., and Saiz-Lopez, A.: A gas-to-particle conversion mechanism helps to explain atmospheric particle formation through clustering of iodine oxides, Nat. Commun., 11, 4521, https://doi.org/10.1038/s41467-020-18252-8, 2020.

Gómez Martín, J. C., Lewis, T. R., James, A. D., Saiz-Lopez, A., and Plane, J. M. C.: Insights into the Chemistry of Iodine New Particle Formation: The Role of Iodine Oxides and the Source of Iodic Acid, J. Am. Chem. Soc., 144, 9240–9253, https://doi.org/10.1021/jacs.1c12957, 2022.

He, X. C., Tham, Y. J., Dada, L., Wang, M., Finkenzeller, H., Stolzenburg, D., Iyer, S., Simon, M., Kurten, A., Shen, J., Rorup, B., Rissanen, M., Schobesberger, S., Baalbaki, R., Wang, D. S., Koenig, T. K., Jokinen, T., Sarnela, N., Beck, L. J., Almeida, J., Amanatidis, S., Amorim, A., Ataei, F., Baccarini, A., Bertozzi, B., Bianchi, F., Brilke, S., Caudillo, L., Chen, D., Chiu, R., Chu, B., Dias, A., Ding, A., Dommen, J., Duplissy, J., El Haddad, I., Gonzalez Carracedo, L., Granzin, M., Hansel, A., Heinritzi, M., Hofbauer, V., Junninen, H., Kangasluoma, J., Kemppainen, D., Kim, C., Kong, W., Krechmer, J. E., Kvashin, A., Laitinen, T., Lamkaddam, H., Lee, C. P., Lehtipalo, K., Leiminger, M., Li, Z., Makhmutov, V., Manninen, H. E., Marie, G., Marten, R., Mathot, S., Mauldin, R. L., Mentler, B., Mohler, O., Muller, T., Nie, W., Onnela, A., Petaja, T., Pfeifer, J., Philippov, M., Ranjithkumar, A., Saiz-Lopez, A., Salma, I., Scholz, W., Schuchmann, S., Schulze, B., Steiner, G., Stozhkov, Y., Tauber, C., Tome, A., Thakur, R. C., Vaisanen, O., Vazquez-Pufleau, M., Wagner, A. C., Wang, Y., Weber, S. K., Winkler, P. M., Wu, Y., Xiao, M., Yan, C., Ye, Q., Ylisirnio, A., Zauner-Wieczorek, M., Zha, Q., Zhou, P., Flagan, R. C., Curtius, J., Baltensperger, U., Kulmala, M., Kerminen, V. M., Kurten, T., Donahue, N. M., Volkamer, R., Kirkby, J., Worsnop, D. R., and Sipila, M.: Role of iodine oxoacids in atmospheric aerosol nucleation, Science, 371, 589–595, https://doi.org/10.1126/science.abe0298, 2021.

Heard, D. E., Read, K. A., Methven, J., Al-Haider, S., Bloss, W. J., Johnson, G. P., Pilling, M. J., Seakins, P. W., Smith, S. C., Sommariva, R., Stanton, J. C., Still, T. J., Ingham, T., Brooks, B., De Leeuw, G., Jackson, A. V., McQuaid, J. B., Morgan, R., Smith, M. H., Carpenter, L. J., Carslaw, N., Hamilton, J., Hopkins, J. R., Lee, J. D., Lewis, A. C., Purvis, R. M., Wevill, D. J., Brough, N., Green, T., Mills, G., Penkett, S. A., Plane, J. M. C., Saiz-Lopez, A., Worton, D., Monks, P. S., Fleming, Z., Rickard, A. R., Alfarra, M. R., Allan, J. D., Bower, K., Coe, H., Cubison, M., Flynn, M., McFiggans, G., Gallagher, M., Norton, E. G., O'Dowd, C. D., Shillito, J., Topping, D., Vaughan, G., Williams, P., Bitter, M., Ball, S. M., Jones, R. L., Povey, I. M., O'Doherty, S., Simmonds, P. G., Allen, A., Kinnersley, R. P., Beddows, D. C. S., Dall'Osto, M., Harrison, R. M., Donovan, R. J., Heal, M. R., Jennings, S. G., Noone, C., and Spain, G.: The North Atlantic Marine Boundary Layer Experiment(NAMBLEX). Overview of the campaign held at Mace Head, Ireland, in summer 2002, Atmos. Chem. Phys., 6, 2241–2272, https://doi.org/10.5194/acp-6-2241-2006, 2006.

Huang, R.-J., Hoffmann, T., Ovadnevaite, J., Laaksonen, A., Kokkola, H., Xu, W., Xu, W., Ceburnis, D., Zhang, R., Seinfeld, J. H., and O'Dowd, C.: Heterogeneous iodine-organic chemistry fast-tracks marine new particle formation, P. Natl. Acad. Sci. USA, 119, e2201729119, https://doi.org/10.1073/pnas.2201729119, 2022.

Inomata, S., Sato, K., Hirokawa, J., Sakamoto, Y., Tanimoto, H., Okumura, M., Tohno, S., and Imamura, T.: Analysis of secondary organic aerosols from ozonolysis of isoprene by proton transfer reaction mass spectrometry, Atmos. Environ., 97, 397–405, https://doi.org/10.1016/j.atmosenv.2014.03.045, 2014.

Jimenez, J. L., Bahreini, R., Cocker III, D. R., Zhuang, H., Varutbangkul, V., Flagan, R. C., Seinfeld, J. H., O'Dowd, C. D., and Hoffmann, T.: New particle formation from photooxidation of diiodomethane (CH_2I_2), J. Geophys. Res.-Atmos., 108, 4318, https://doi.org/10.1029/2002JD002452, 2003.

Kundu, S., Fisseha, R., Putman, A. L., Rahn, T. A., and Mazzoleni, L. R.: High molecular weight SOA formation during limonene ozonolysis: insights from ultrahigh-resolution FT-ICR mass spectrometry characterization, Atmos. Chem. Phys., 12, 5523–5536, https://doi.org/10.5194/acp-12-5523-2012, 2012.

Kundu, S., Fisseha, R., Putman, A. L., Rahn, T. A., and Mazzoleni, L. R.: Molecular formula composition of β-caryophyllene ozonolysis SOA formed in humid and dry conditions, Atmos. Environ., 154, 70–81, https://doi.org/10.1016/j.atmosenv.2016.12.031, 2017.

Li, R., Palm, B. B., Ortega, A. M., Hlywiak, J., Hu, W., Peng, Z., Day, D. A., Knote, C., Brune, W. H., de Gouw, J. A., and Jimenez, J. L.: Modeling the Radical Chemistry in an Oxidation Flow Reactor: Radical Formation and Recycling, Sensitivities, and the OH Exposure Estimation Equation, J. Phys. Chem. A, 119, 4418–4432, https://doi.org/10.1021/jp509534k, 2015.

Lopez-Hilfiker, F. D., Mohr, C., Ehn, M., Rubach, F., Kleist, E., Wildt, J., Mentel, Th. F., Lutz, A., Hallquist, M., Worsnop, D., and Thornton, J. A.: A novel method for online analysis of gas and particle composition: description and evaluation of a Filter Inlet for Gases and AEROsols (FIGAERO), Atmos. Meas. Tech., 7, 983–1001, https://doi.org/10.5194/amt-7-983-2014, 2014.

McFiggans, G., Coe, H., Burgess, R., Allan, J., Cubison, M., Alfarra, M. R., Saunders, R., Saiz-Lopez, A., Plane, J. M. C., Wevill, D., Carpenter, L., Rickard, A. R., and Monks, P. S.: Direct evidence for coastal iodine particles from Laminaria macroalgae – linkage to emissions of molecular iodine, Atmos. Chem. Phys., 4, 701–713, https://doi.org/10.5194/acp-4-701-2004, 2004.

McFiggans, G., Bale, C. S. E., Ball, S. M., Beames, J. M., Bloss, W. J., Carpenter, L. J., Dorsey, J., Dunk, R., Flynn, M. J., Furneaux, K. L., Gallagher, M. W., Heard, D. E., Hollingsworth, A. M., Hornsby, K., Ingham, T., Jones, C. E., Jones, R. L., Kramer, L. J., Langridge, J. M., Leblanc, C., LeCrane, J.-P., Lee, J. D., Leigh, R. J., Longley, I., Mahajan, A. S., Monks, P. S., Oetjen, H., Orr-Ewing, A. J., Plane, J. M. C., Potin, P., Shillings, A. J. L., Thomas, F., von Glasow, R., Wada, R., Whalley, L. K., and Whitehead, J. D.: Iodine-mediated coastal particle formation: an overview of the Reactive Halogens in the Marine Boundary Layer (RHaMBLe) Roscoff coastal study, Atmos. Chem. Phys., 10, 2975–2999, https://doi.org/10.5194/acp-10-2975-2010, 2010.

Monahan, C., Ashu-Ayem, E. R., Nitschke, U., Darby, S. B., Smith, P. D., Stengel, D. B., Venables, D. S., and O'Dowd,

C. D.: Coastal Iodine Emissions: Part 2. Chamber Experiments of Particle Formation from Laminaria digitata-Derived and Laboratory-Generated I2, Environ. Sci. Technol., 46, 10422–10428, https://doi.org/10.1021/es3011805, 2012.

Nguyen, T. B., Bateman, A. P., Bones, D. L., Nizkorodov, S. A., Laskin, J., and Laskin, A.: High-resolution mass spectrometry analysis of secondary organic aerosol generated by ozonolysis of isoprene, Atmos. Environ., 44, 1032–1042, https://doi.org/10.1016/j.atmosenv.2009.12.019, 2010.

O'Dowd, C. D., Jimenez, J. L., Bahreini, R., Flagan, R. C., Seinfeld, J. H., Hämeri, K., Pirjola, L., Kulmala, M., Jennings, S. G., and Hoffmann, T.: Marine aerosol formation from biogenic iodine emissions, Nature, 417, 632, https://doi.org/10.1038/nature00775, 2002.

O'Dowd, C. D., Facchini, M. C., Cavalli, F., Cebrunis, D., Mircea, M., Decesari, S., Fuzzi, S., Yoon, Y. J., and Putard, J.-P.: Biogenically driven organic contribution to marine aerosol, Nature, 431, 676–680, 2004.

Plane, J. M. C., Joseph, D. M., Allan, B. J., Ashworth, S. H., and Francisco, J. S.: An Experimental and Theoretical Study of the Reactions OIO + NO and OIO + OH, J. Phys. Chem. A, 110, 93–100, https://doi.org/10.1021/jp055364y, 2006.

Putman, A. L., Offenberg, J. H., Fisseha, R., Kundu, S., Rahn, T. A., and Mazzoleni, L. R.: Ultrahigh-resolution FT-ICR mass spectrometry characterization of α-pinene ozonolysis SOA, Atmos. Environ., 46, 164–172, https://doi.org/10.1016/j.atmosenv.2011.10.003, 2012.

Riva, M., Budisulistiorini, S. H., Zhang, Z. F., Gold, A., Thornton, J. A., Turpin, B. J., and Surratt, J. D.: Multiphase reactivity of gaseous hydroperoxide oligomers produced from isoprene ozonolysis in the presence of acidified aerosols, Atmos. Environ., 152, 314–322, https://doi.org/10.1016/j.atmosenv.2016.12.040, 2017.

Saiz-Lopez, A., Plane, J. M. C., Baker, A. R., Carpenter, L. J., von Glasow, R., Gómez Martín, J. C., McFiggans, G., and Saunders, R. W.: Atmospheric Chemistry of Iodine, Chem. Rev., 112, 1773–1804, https://doi.org/10.1021/cr200029u, 2012.

Saiz-Lopez, A., Fernandez, R. P., Ordóñez, C., Kinnison, D. E., Gómez Martín, J. C., Lamarque, J.-F., and Tilmes, S.: Iodine chemistry in the troposphere and its effect on ozone, Atmos. Chem. Phys., 14, 13119–13143, https://doi.org/10.5194/acp-14-13119-2014, 2014.

Saunders, R. W. and Plane, J. M. C.: Formation Pathways and Composition of Iodine Oxide Ultra-Fine Particles, Environ. Chem., 2, 299–303, https://doi.org/10.1071/EN05079, 2005.

Saunders, R. W., Kumar, R., Gómez Martín, J. C., Mahajan, A. S., Murray, B. J. and Plane, J. M. C.: Studies of the Formation and Growth of Aerosol from Molecular Iodine Precursor, Z. Phys. Chem., 224, 1095–1117, https://doi.org/10.1524/zpch.2010.6143, 2010.

Seinfeld, J. H. and Pandis, S. N.: Atmospheric chemistry and physics: from air pollution to climate change, 3nd, John Wiley and Sons. Inc., New York, ISBN 978-1-119-22117-3, 2016.

Sellegri, K., Yoon, Y. J., Jennings, S. G., O'Dowd, C. D., Pirjola, L., Cautenet, S., Chen, H., and Hoffmann, T.: Quantification of Coastal New Ultra-Fine Particles Formation from In situ and Chamber Measurements during the BIOFLUX Campaign, Environ. Chem., 2, 260–270, https://doi.org/10.1071/EN05074, 2005.

Sellegri, K., Pey, J., Rose, C., Culot, A., DeWitt, H. L., Mas, S., Schwier, A. N., Temime-Roussel, B., Charriere, B., Saiz-Lopez, A., Mahajan, A. S., Parin, D., Kukui, A., Sempere, R., D'Anna, B., and Marchand, N.: Evidence of atmospheric nanoparticle formation from emissions of marine microorganisms, Geophys. Res. Lett., 43, 6596–6603, https://doi.org/10.1002/2016GL069389, 2016.

Sipilä, M., Sarnela, N., Jokinen, T., Henschel, H., Junninen, H., Kontkanen, J., Richters, S., Kangasluoma, J., Franchin, A., Peräkylä, O., Rissanen, M. P., Ehn, M., Vehkamäki, H., Kurten, T., Berndt, T., Petäjä, T., Worsnop, D., Ceburnis, D., Kerminen, V.-M., Kulmala, M., and O'Dowd, C.: Molecular-scale evidence of aerosol particle formation via sequential addition of HIO_3, Nature, 537, 532–534, https://doi.org/10.1038/nature19314, 2016.

Teruel, M. A., Dillon, T. J., Horowitz, A., and Crowley, J. N.: Reaction of $O(^3P)$ with the alkyl iodides: CF_3I, CH_3I, CH_2I_2, C_2H_5I, 1-C_3H_7I and 2-C_3H_7I, Phys. Chem. Chem. Phys., 6, 2172–2178, https://doi.org/10.1039/B316402K, 2004.

Vaattovaara, P., Huttunen, P. E., Yoon, Y. J., Joutsensaari, J., Lehtinen, K. E. J., O'Dowd, C. D., and Laaksonen, A.: The composition of nucleation and Aitken modes particles during coastal nucleation events: evidence for marine secondary organic contribution, Atmos. Chem. Phys., 6, 4601–4616, https://doi.org/10.5194/acp-6-4601-2006, 2006.

Wang, M., Zeng, L., Lu, S., Shao, M., Liu, X., Yu, X., Chen, W., Yuan, B., Zhang, Q., Hu, M., and Zhang, Z.: Development and validation of a cryogen-free automatic gas chromatograph system (GC-MS/FID) for online measurements of volatile organic compounds, Analytical Methods, 6, 9424–9434, https://doi.org/10.1039/C4AY01855A, 2014.

Wang, M., Chen, D., Xiao, M., Ye, Q., Stolzenburg, D., Hofbauer, V., Ye, P., Vogel, A. L., Mauldin, R. L., 3rd, Amorim, A., Baccarini, A., Baumgartner, B., Brilke, S., Dada, L., Dias, A., Duplissy, J., Finkenzeller, H., Garmash, O., He, X. C., Hoyle, C. R., Kim, C., Kvashnin, A., Lehtipalo, K., Fischer, L., Molteni, U., Petäjä, T., Pospisilova, V., Quéléver, L. L. J., Rissanen, M., Simon, M., Tauber, C., Tomé, A., Wagner, A. C., Weitz, L., Volkamer, R., Winkler, P. M., Kirkby, J., Worsnop, D. R., Kulmala, M., Baltensperger, U., Dommen, J., El-Haddad, I., and Donahue, N. M.: Photo-oxidation of Aromatic Hydrocarbons Produces Low-Volatility Organic Compounds, Environ. Sci. Technol., 54, 7911–7921, https://doi.org/10.1021/acs.est.0c02100, 2020.

Wang, X., Hayeck, N., Brüggemann, M., Yao, L., Chen, H., Zhang, C., Emmelin, C., Chen, J., George, C., and Wang, L.: Chemical Characteristics of Organic Aerosols in Shanghai: A Study by Ultrahigh-Performance Liquid Chromatography Coupled With Orbitrap Mass Spectrometry, J. Geophys. Res.-Atmos., 122, 11703–711722, https://doi.org/10.1002/2017JD026930, 2017.

Whitehead, J. D., McFiggans, G. B., Gallagher, M. W., and Flynn, M. J.: Direct linkage between tidally driven coastal ozone deposition fluxes, particle emission fluxes, and subsequent CCN formation, Geophys. Res. Lett., 36, L04806, https://doi.org/10.1029/2008GL035969, 2009.

Yan, C., Nie, W., Vogel, A. L., Dada, L., Lehtipalo, K., Stolzenburg, D., Wagner, R., Rissanen, M. P., Xiao, M., Ahonen, L., Fischer, L., Rose, C., Bianchi, F., Gordon, H., Simon, M., Heinritzi, M., Garmash, O., Roldin, P., Dias, A., Ye, P., Hofbauer, V., Amorim, A., Bauer, P. S., Bergen, A., Bernhammer, A. K., Breitenlech-

ner, M., Brilke, S., Buchholz, A., Mazon, S. B., Canagaratna, M. R., Chen, X., Ding, A., Dommen, J., Draper, D. C., Duplissy, J., Frege, C., Heyn, C., Guida, R., Hakala, J., Heikkinen, L., Hoyle, C. R., Jokinen, T., Kangasluoma, J., Kirkby, J., Kontkanen, J., Kürten, A., Lawler, M. J., Mai, H., Mathot, S., Mauldin, R. L., 3rd, Molteni, U., Nichman, L., Nieminen, T., Nowak, J., Ojdanic, A., Onnela, A., Pajunoja, A., Petäjä, T., Piel, F., Quéléver, L. L. J., Sarnela, N., Schallhart, S., Sengupta, K., Sipilä, M., Tomé, A., Tröstl, J., Väisänen, O., Wagner, A. C., Ylisirniö, A., Zha, Q., Baltensperger, U., Carslaw, K. S., Curtius, J., Flagan, R. C., Hansel, A., Riipinen, I., Smith, J. N., Virtanen, A., Winkler, P. M., Donahue, N. M., Kerminen, V. M., Kulmala, M., Ehn, M., and Worsnop, D. R.: Size-dependent influence of NO_x on the growth rates of organic aerosol particles, Science Advances, 6, eaay4945, https://doi.org/10.1126/sciadv.aay4945, 2020.

Yu, H.: Size spectrum, time series and atom number distribution of macroalgal emission vapors and oxidation products, Zenodo [data set], https://doi.org/10.5281/zenodo.6965859, 2022.

Yu, H., Ren, L., Huang, X., Xie, M., He, J., and Xiao, H.: Iodine speciation and size distribution in ambient aerosols at a coastal new particle formation hotspot in China, Atmos. Chem. Phys., 19, 4025–4039, https://doi.org/10.5194/acp-19-4025-2019, 2019.